RSC Advances

ROYAL SOCIETY OF CHEMISTRY

www.rsc.org/advances

RSC Advances

ARTICLE

Ultrafine SnO_2 nanoparticles decorated onto graphene for high performance lithium storage

Received 00th January 20xx,
Accepted 00th January 20xx

DOI: 10.1039/x0xx00000x

www.rsc.org/

Huijuan Zhang[a], Lijun Gao[a]*,Shubin Yang[b]*

Ultrafine SnO_2 nanoparticles of 2-5 nm are controllably synthesized onto the surface of graphene via a simple one-pot hydrothermal approach without the addition of surfactant. The resulting SnO_2-graphene nanocomposite shows a high level of homogenerous dispersion and high content of nano-sized SnO_2 (85 %) loading. Such unique features of SnO_2-graphene nanocomposite can not only buffer efficiently the volume change of SnO_2 during charge-discharge processes, but also facilitate fast diffusion of lithium ions in SnO_2 and transport of electrons in graphene when it is used as anode material for lithium storage. As a result, ultrafine SnO_2-graphene nanocomposite exhibits a very high reversible capacity of 1037 mAh g^{-1}, excellent capacity retention of 90% over 150 cycles, and good high-rate capability. Combined with other advantages of easy synthesis, low-cost, environmental friendliness and high yield, the SnO_2-graphene nanocomposite could be a promising anode material for lithium ion batteries

Introduction

Lithium ion batteries have become one of the most promising power sources for electronics and electric vehicles owing to their high energy density. Although graphitic carbons have been commercially available as anode materials for lithium ion batteries, they are limited by their low theoretical capacity (372 mAh g^{-1}). It is urgently required to develop new anode materials with high capacities for lithium storage. Thus, electrochemically active metal oxides such as SnO_2, CuO, Fe_3O_4, Co_3O_4 have recently attracted much attention due to their high theoretical capacities (～1000 mAh g^{-1}) [1-10]. In particular, SnO_2 is abundant, non-toxic, and inexpensive, holding a great promise for use in lithium ion batteries.

Despite of above advantages, SnO_2 also suffers from large volume changes and agglomeration associated with lithium insertion and extraction processes, which result in the loss of electrical contact between particles in anode and rapid capacity decay [3, 11-15]. To circumvent these issues, one efficient strategy is to incorporate SnO_2 with carbonaceous materials to prepare SnO_2-carbon hybrids, in which carbon can not only buffer the volume change of SnO_2 but also improve the electrical conductivity of the electrode. Until now, various types of carbon including graphite, mesoporous or macroporous carbons, carbon nanotubes and graphene have been widely selected as supporting matrixes for SnO_2 [12, 13, 16]. Especially, single-layer graphene, with many unique properties such as high surface area, superior electronic conductivity and good flexibility[17-19], has been studied to composite with SnO_2 [20, 21]. In this regard, SnO_2 nanorods/graphene [22], SnO_2 nanoparticles/reduced graphene oxide [15, 23, 24], SnO_2 nanoparticles confined in a graphene framework [25], 3D graphene supported SnO_2 nanoparticles [26-28] and sandwich-like SnO_2-graphene hybrids [29] have been achieved, and these composites all showed improved electrochemical performances for lithium storage. Moreover, it is found that the reversible capacities and cycle stabilities of the SnO_2/graphene hybrids are strongly dependent on the dispersion level and particle size of SnO_2 in the composites. The small size and well dispersion of SnO_2 particles onto graphene are the key factors enabling high capacities and good high-rate performances of the composites. However, in most cases, the size of SnO_2 nanocrystals in SnO_2/graphene composites is in the range of 10 nm to 100 nm, and they are usually in homogeneously dispersed on graphene layers. Furthermore, during the synthesis processes, adoption of surfactants are necessary to avoid aggregation of graphene sheets or/and SnO_2 nanocrystals.

In this work, ultrafine SnO_2 nanoparticles are controllably grown onto the surface of graphene via a simple one-pot hydrothermal approach without any addition of surfactant. The as-prepared SnO_2/graphene nanocomposites have particle size of 2-5 nm, high level of homogeneous dispersion and high content of SnO_2 (85 %). Such unique features can not only diminish efficiently the volume change of SnO_2 during the charge-discharge processes, but also facilitate fast diffusion of lithium ions as they are used as anode material for lithium storage. The resulting SnO_2/graphene nanocomposite exhibits a very high reversible capacity of 1037 mAh g^{-1}, excellent capacity retention of 91 % over 80 cycles, and good high-rate capability of 320 mAh g^{-1} at a high rate of 800 mA g^{-1}.

[a] School of Energy, College of Physics, Optoelectronics and Energy & Collaborative Innovation Center of Suzhou Nano Science and Technology, Soochow University, Suzhou 215006, China. E-mail: gaolijun@suda.edu.cn, Tel.:+86 512 65229905
[b] School of Materials Science and Engineering, Beihang University, Beijing 100191, China. E-mail: yangshubin@buaa.edu.cn

Experimental

Synthesis of ultrafine SnO_2/Graphene composites: Graphene oxide (GO) nanosheets were prepared by using a modified Hummers' method from flake graphite as reported previously [30-32]. In a typical experiment, 7 g tin dichloride dehydrate ($SnCl_2{\cdot}2H_2O$) was dissolved in 50 ml distilled water. Under probe sonication, 20 ml GO suspension (6.56 mg/ml) was added dropwise into above solution. And then the pH value of as-prepared $SnCl_2$-GO suspensions were adjusted from 0.2 to 9.5 by adding a certain amount of HCl or NH_3, and then sonicated for 1 h before being transferred to a Teflon-lined stainless steel autoclave, and subsequently heated at 180 °C for 12 h. Black fluffy products (SnO_2-GO) were harvested after freeze-drying for overnight. Afterward, the as-prepared products were thermally reduced at 400 °C in a horizontal furnace under N_2 atmosphere for 2 h, producing various nano-sized SnO_2 particles decorated graphene (denoted as SnO_2-G-400, pH=*X*, *X*=0.2, 1.0, 2.4, 9.5). Notably, SnO_2-G-400 was represented as SnO_2-G-400 when pH=1.0. For comparison, pure SnO_2 nanoparticles were also prepared via the same conditions without the addition of GO dispersion.

Materials Characterization: The morphology and microstructure of the samples were systematically investigated by scanning electron microscope (SEM, JEOL JSM-6700F), transmission electron microscopy (TEM) and high-resolution TEM (HRTEM, Field Emission JEOL 2100F), EDX (energy dispersive x-ray spectroscopy), X-ray diffraction (XRD, X-ray diffractometer Rigaku D/Max 2200), Raman (Jobin-Yvon Labor Raman HR-800) and X-ray photoelectron spectroscopy (XPS, KRATOS AXIS ULTRA-DLD). The thermogravimetric analysis (TGA, NETZSCH Jupiter STA 449 F3) was carried out in air atmosphere up to 800°C.

Electrochemical Measurements: Electrochemical experiments were carried out using 2032 coin-type cells. The working electrodes were prepared by mixing the active material, acetylene black and poly(vinyl difluoride) (PVDF) at a weight ratio of 80:10:10 and pasted on pure Ni foam, pure lithium foil was used as the counter electrode for lithium ion battery. The electrolyte consisted of a solution of 1 M $LiPF_6$ in ethylene carbonate (EC)/dimethyl carbonate (DMC)/diethyl carbonate (DEC) (1:1:1 by volume) obtained from MTI Corporation. Celgard 2400 membrane was used as the separator. The cells were assembled in an argon-filled glove box with the concentrations of moisture and oxygen below 0.1 ppm. The electrochemical performances were tested at various current densities in the voltage range of 0.01–3.0 V on a LANDct3.3 battery tester. The electrochemical impedance spectroscopy (EIS, CHI760E) measurements were recorded by applying a sine wave with amplitude of 5.0 mV over the frequency range from 100 kHz to 0.1 Hz. Fitting of impedance spectra to the proposed equivalent circuit was performed by the code Zview.

Results and discussion

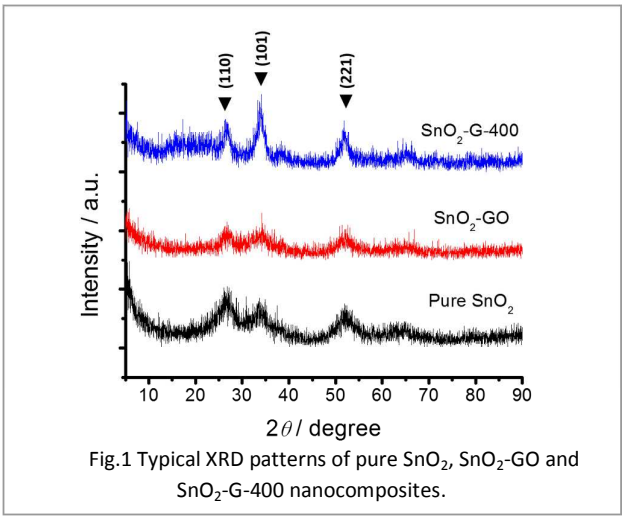

Fig.1 Typical XRD patterns of pure SnO_2, SnO_2-GO and SnO_2-G-400 nanocomposites.

The as-prepared pure SnO_2, SnO_2-GO and SnO_2-G-400 nanocomposites were firstly identified by X-ray diffraction (XRD) patterns. As displayed in Fig.1, there are four diffraction peaks at 26.6°, 33.5°, and 51.5°, corresponding to the (110), (101) and (211) and facets of tetragonal SnO_2 with cassiterite structure (JCPDS no. 41-1445), respectively. It is obvious that all the diffraction peaks are broad and weak in intensities, indicating that the sizes of the SnO_2 particles are very small. There is no obvious characteristic peak of stacked graphene at 25° in the XRD patterns of SnO_2-G-400 nanocomposite, suggesting that graphene sheets are uniformly dispersed in the composites during fabrication processes.[33, 34] Notably, after thermal treatment at 400°C, the peak intensities of SnO_2-G-400 only increase slightly in comparison with those of SnO_2-GO, indicating that the SnO_2 material is stable at the 400 °C high temperatures.

The SnO_2-G-400 composite was also characterized by Raman spectroscopy as shown in Fig. 2. The peaks at about 1323 and 1591 cm^{-1} are assigned to the D and G band of graphene, respectively, and the intensity ratio of the D to G band (I_D/I_G) is 1.3, which is lower than that of graphene oxide (1.5)[35], indicating that oxygen functional groups on the surface of graphene have been partially

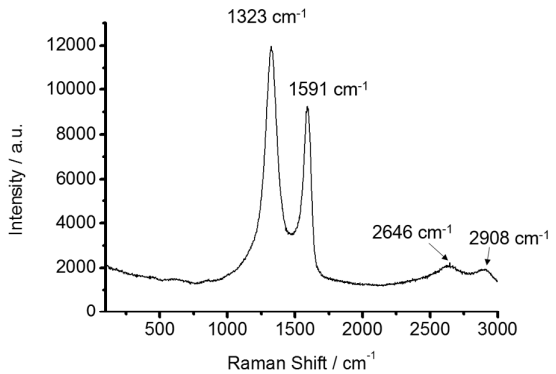

Fig.2 Raman spectrum of SnO_2-G-400 nanocomposite

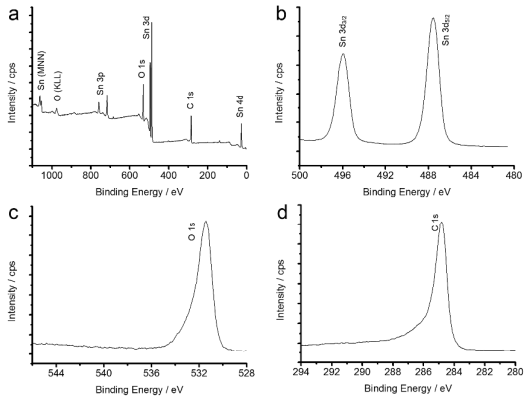

Fig.3 (a) XPS survey spectrum of SnO_2-G-400, high resolution spectra peaks of (b) Sn3d, (c) O1s and (d) C1s

removed during the thermal treatment process at 400°C in N_2. The peaks at about 2676 and 2929 cm^{-1} are assigned to the 2D and D + G band of single-layer graphene, respectively, further demonstrating the removal of oxygen containing functional groups after thermal treatment. In order to investigate the surface composition and chemical states of SnO_2-G-400, XPS analysis was conducted in the range of 0-1100 eV. As shown in Fig.3a, Sn3d, O1s and C1s can be clearly seen in the wide survey XPS spectrum. The atomic ratio of Sn and O is about 1:2, suggesting the presence of a great amount of SnO_2 in the composite. The high-resolution spectra of Sn3d (Fig. 3b) peaks are perfectly symmetric, clearly demonstrating the presence of pure SnO_2 in the composite, in good agreement with the analysis result from XRD (Fig. 1).

To elucidate the morphology and microstructure of SnO_2-G-400 nanocomposite, scanning electron microscopy (SEM) and transmission electron microscopy (TEM) measurements were carried out. As shown in Fig. 4a and 4b, a large quantity of nanoparticles are uniformly dispersed onto/into the graphene layers to form compact composites as large as several micrometers. The typical HRTEM image (Fig. 4c) reveals that the diameters of these nanoparticles are in the range of 2-5 nm (Fig. 4e). The typical EDX elemental analysis (Fig. 4d) reveals the presence of Sn, C, O and Cu elements in the SnO_2-G-400 composites, where Sn and O should be resulted from the SnO_2, C from graphene and Cu from the TEM grid. The selected area electron diffraction (SAED) pattern of these nanoparticles in the composite presents obvious spot rings, which correspond to the lattice spacing of SnO_2, in good agreement with the XRD analysis. Thermogravimetric analysis (TGA) of SnO_2-G-400 reveals that the weight content of SnO_2 in the composite is 85 %, as shown in Fig. 4f. The distribution of SnO_2 in the composite can be further unravelled by element mapping images of C, Sn and O, as shown in Fig.5, it is clear that C, Sn and O are homogeneously distributed onto the graphene, which is consistent with the TEM observation. Such a high content of SnO_2 nanoparticles with a uniform dispersion should result in high capacity when the SnO_2-G-400 nanocomposite is used as an anode material for lithium ion battery.

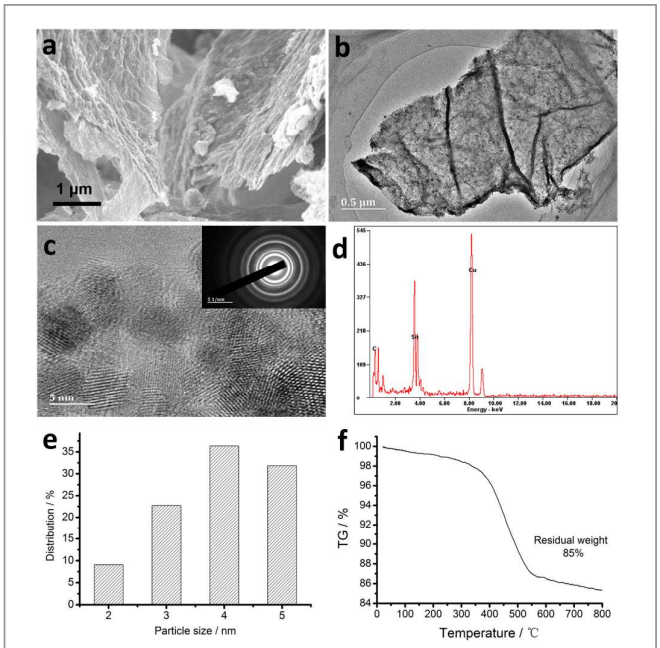

Fig.4 (a) FE-SEM, (b) TEM, (c) HRTEM images and (d) EDX elemental analysis of SnO_2-G-400 nanocomposite, (e) size distribution of SnO_2 calculated from HRTEM images, and (f) TGA results for SnO_2-G-400 nanocomposites.

Galvanostatic discharge-charge experiments were carried out to evaluate the electrochemical performances of SnO_2-G-400 nanocomposite. For comparison, pure SnO_2 nanoparticles and SnO_2-GO composites were also tested under the same electrochemical conditions. The selected discharge-charge profiles of pure SnO_2, SnO_2-GO and SnO_2-G-400 nanocomposites at a current density of 100 mA g^{-1} are presented in Figure 6a-c, respectively. It is remarkable to note that a very high reversible capacity of 1037 mAh g^{-1} for SnO_2-G-400 in the voltage range from 0.01 to 3.00 V is achieved, which is three times higher than that of graphite (~300 mAh g^{-1}) and higher than those of pure SnO_2 (840 mAh g^{-1}) and SnO_2-GO (881 mAh g^{-1}). Notably, the capacity of SnO_2-G-400 composite is higher than the theoretical capacity of single SnO_2 and/or graphene, suggesting that there are other lithium storage mechanisms, except for the classic lithium storage mechanisms in SnO_2 and graphene layers. From the charge-discharge curves of SnO_2-G-400 composite (Fig.6c), it is observed that in the case of charging voltage above 1.5V, there is still a high reversible capacity of about 300 mAh g^{-1}. This phenomenon is similar to those reports on nanostructured carbons or metal oxides with high surface areas and multi-sized pores, in which an additional surface and porous storage mechanism exist. Thereby, we believe that such surface and porous lithium storage combined with the classic storage of SnO_2 gives rise to a very high capacity of more than 1000 mAh g^{-1} for SnO_2-G-400 composite as anode material for lithium storage[15, 36]. The electrochemical activity of SnO_2-G-400 for lithium storage was further evaluated by cyclic voltammetry (CV) over the potential range of 0.01 V - 3.0 V at a scan rate of 0.2 mV s^{-1}. As shown in Fig. 5d, there is a broad cathodic peak from 1.0 V to 0.5 V during the

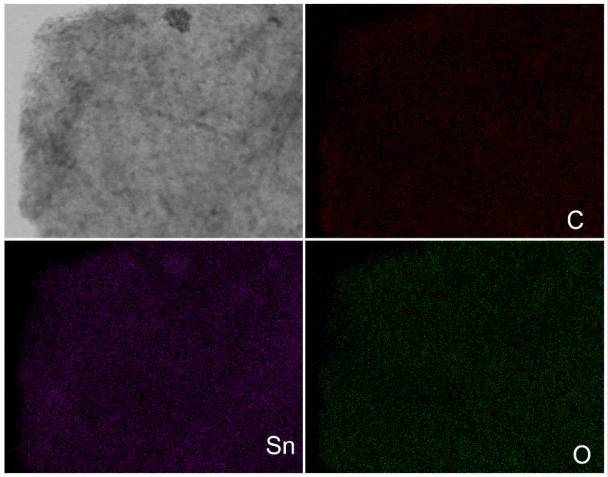

Fig.5 C, Sn, O elemental mapping images of SnO_2-G-400.

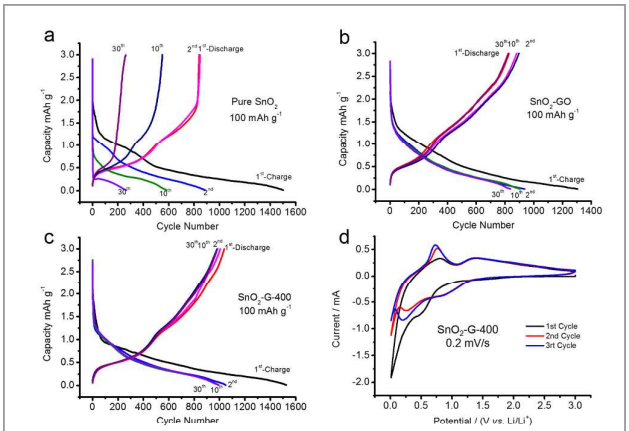

Fig. 6 Charge and discharge cycle profiles of (a) pure SnO_2, (b) SnO_2-GO and (c) SnO_2-G-400 at current density of 100 mA g^{-1}, (d) first three scanning CV profiles of SnO_2-G-400 at a scan rate of 0.2 mV s^{-1}

first scanning process, which can be ascribed to the formation of solid electrolyte interface (SEI) layer at the surface of active materials as well as the reduction of SnO_2 to Sn with the synchronous formation of Li_2O. During the first scanning process, the oxidation peak from 0.5 V to 0.9 V can be explained as the Li^+ extraction from graphene layers and the lithium de-alloying from Li_xSn. The other oxidation peak around 1.25 V - 1.75 V can be attributed to a conversion reaction between Li_2O and metallic Sn.[15]

In addition, the SnO_2-G-400 nanocomposite delivers a first coulombic efficiency of 67.9%, which is higher than those of SnO_2-GO (63.5 %). This should ascribe to the additional irreversible side reaction with residual functional groups that exist on the GO layers for SnO_2-GO sample, except for the formation of Li_2O and solid-electrolyte interface (SEI) layers. During the subsequent cycles, the coulombic efficiencies of both SnO_2-G-400 and SnO_2-GO are increased to nearly 100 % (Fig. 7a).The cycle performances and high-rate properties of pure SnO_2, SnO_2-GO and SnO_2-G-400 nanocomposites are compared in Figure 6b and 6c. It is clear that both of SnO_2-GOand SnO_2-G-400 nanocomposites exhibit excellent capacities of 827 and 942 mAh g^{-1}, respectively, after 80 cycles at a current of 100 mA g^{-1}. Those values are much higher than that of pure SnO_2 nanoparticles (142 mAh g^{-1}), as well as those reported for SnO_2 nanorods-graphene and SnO_2-graphene frameworks (400-800 mAh g^{-1}) [3, 22, 25, 27, 37-39]. At higher charge and discharge rates, the capacity retention of SnO_2-G-400 is more evident. For example, at current densities of 200 and 800 mA g^{-1}, the reversible capacities of SnO_2-G-400 are still as high as 940 and 320 mAh g^{-1}, respectively. These values are in contrast to those of SnO_2-GO and pure SnO_2 nanoparticles which decays to nearly 100 mAh g^{-1} (Fig. 7a). More importantly, the capacity of SnO_2-G-400 can recover to ~900 mAh g^{-1} at the current density of 100 mA g^{-1} and maintains 90 % of its initial capacity after 150 cycles. In order to analyse the reason that leads to high electrochemical performances of SnO_2-G-400 for lithium storage, electrochemical impedance spectroscopy (EIS) measurements of pure SnO_2, SnO_2-GO and SnO_2-G-400 nanocomposites were carried out after 30 cycles. As presented in Fig. 7c, all the EIS spectra exhibit two semi-circles at high frequencies followed by a liner straight line at low frequencies, which can be fitted by the modified Randles equivalent circuit in Fig.7c [40, 41]. Obviously, the film resistance (R_f) and charge-transfer resistance (R_{ct}) of SnO_2-G-400 are 5.07 Ω and 7.29 Ω, respectively, which are much lower than those of SnO_2-GO (6.26 and 10.56 Ω) and pure SnO_2 nanoparticles (10.94 and 32.84 Ω). This result

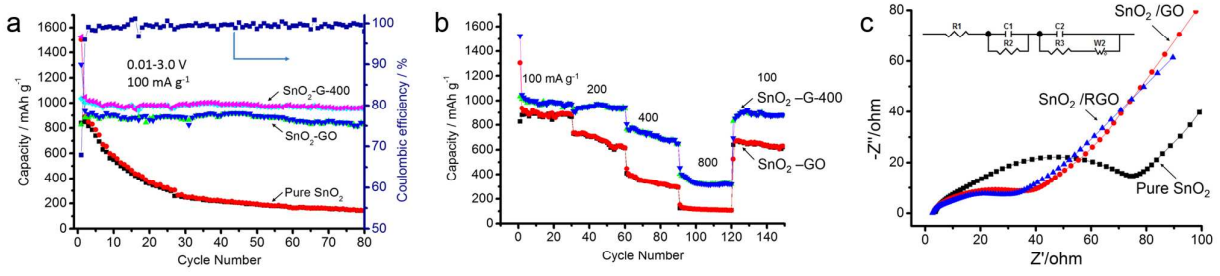

Fig. 7 (a) cycle performance of pure SnO_2, SnO_2-GO and SnO_2-G-400, and coulombic efficiency of SnO_2-G-400 at current density of 100 mA g^{-1}, (b) rate capabilities of SnO_2-GO and SnO_2-G-400, (c) impedance Nyquist plots of pure SnO_2, SnO_2-GO and SnO_2-G-400 after 30 cycles. The inset is the equivalent circuit used for analysis of impedance data.

confirms that the combination of graphene with SnO_2 can not only

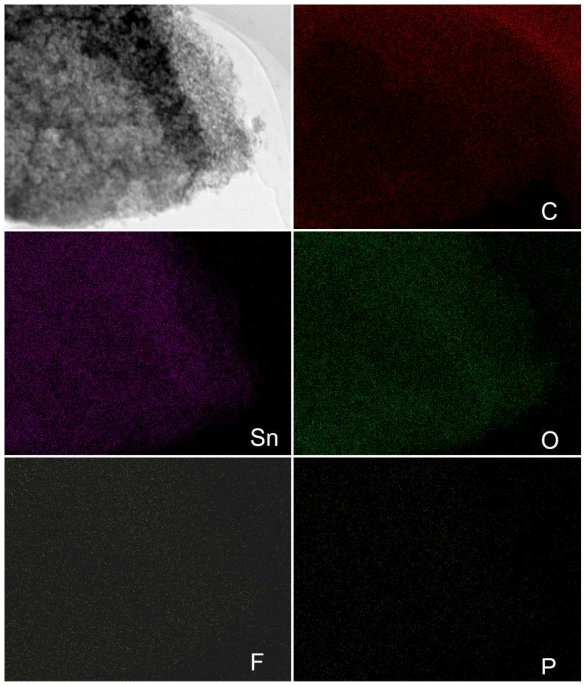

Fig.8 The element mapping of SnO_2-G-400 after 150 cycles, revealing that C, Sn, O, F, P are homogeneously dispersed into the graphene nanosheets.

preserve high conductivity of the overall electrode, but also largely improve electrochemical activity of SnO_2 during the cycle processes.

To further analyse the reason of high performance of SnO_2-G-400 composite for lithium storage, we disassembled the testing cell after 150 cycles and conducted elemental mapping tests again. As shown in Fig.8, it can be clearly seen that C, Sn and O elements are still homogeneously dispersed in the graphene nanosheets, except for the presence of F and P elements from electrolyte. This demonstrates that the morphology and microstructure of the SnO_2-G-400 composite can be well kept even undergoing a long-term charge and discharge cycles. The stable structure leads to the good cycle performance of SnO_2-G-400 for lithium storage. Correspondingly, from the HRTEM image of SnO_2-G-400 composite

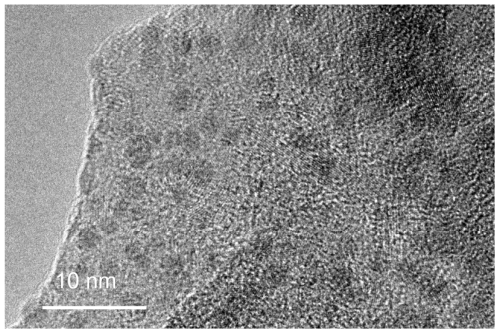

Fig.9. HRTEM image of SnO_2-G-400 electrode after 150 cycles. It can be clearly seen that ultrafine nanoparticles are anchored onto the surface of graphene nanosheets.

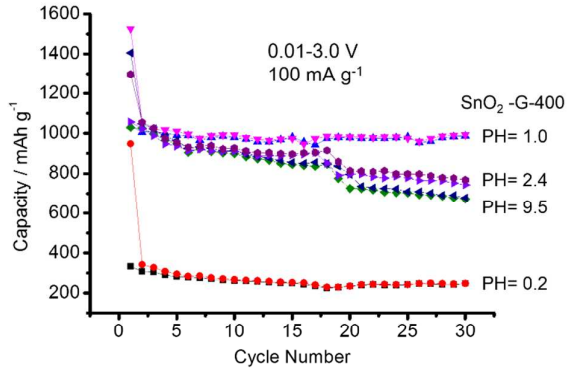

Fig. 10 Cycle performances of SnO_2-G-400 prepared at various pH values.

after 150 cycles (Fig.9), it can be seen that a number of SnO_2 nanoparticles are still anchored onto the surface of graphene, further confirming the good stability of SnO_2-G-400 composite during the cycle processes.

The influence of SnO_2 particle size on electrochemical performance for lithium storage are studied, we manage to tune the size of SnO_2 nanoparticles in SnO_2-G-400 by simply adjusting the pH values from 0.2 to 9.5, which play a key role in controlling the hydrolysis rates of $SnCl_2$ and the size of SnO_2 nanoparticles. The cycle performances of composites with different pH values were compared in Fig.10. The typical TEM images of SnO_2-G-400 samples with pH = 0.2, 2.4 and 9.5 were shown in Fig.11. When the pH value is less than 1.0, the capacity of SnO_2-G-400 is only 332 mAh g^{-1}, which should be attributed to the less extent of formation of SnO_2

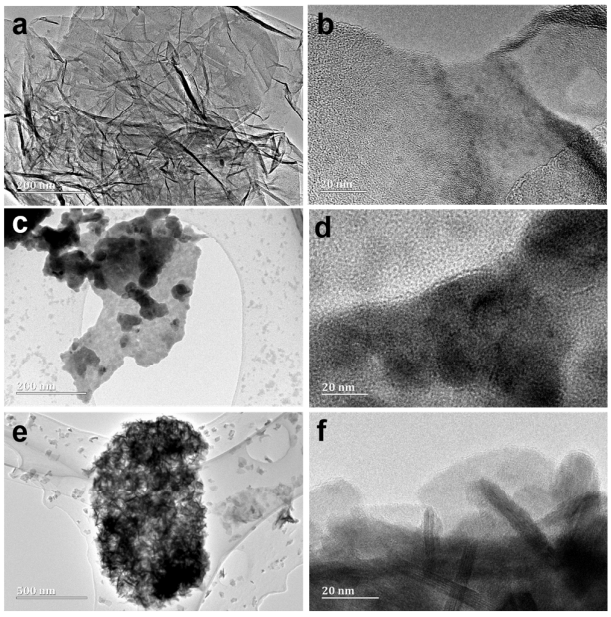

Fig.11 The TEM images of SnO_2-G-400 composites prepared when (a, b) pH=0.2, (c, d) pH=2.4, (e, f) pH=9.5.

on graphene during the fabrication process (Fig.11a, b). As the pH is increased to 1.0, the capacity of SnO_2-G-400 is significantly increased to ~1000 mAh g^{-1}, and it maintains 90 % of the initial capacity after 150 cycles as it is discussed above. However, as the pH is further increased to 2.4 and 9.5, the initial capacities of SnO_2-G-400 are similar to that prepared at pH = 1.0, but the capacities rapidly decrease around 750 mAh g^{-1} after 30 cycles. The poor cycling stability can be attributed to the severe aggregation of SnO_2 nanoparticles on the surface of graphene (pH=2.4 in Fig.11 c, d and pH=9.5 in Fig.11 e, f).These results suggest that both conductive graphene and SnO_2 particle size are crucial for improving the electrochemical performances of SnO_2-graphene composites.

Conclusions

In summary, ultrafine SnO_2 nanoparticles (2-5 nm) decorated on graphene sheets have been successfully fabricated via a simple one-pot hydrothermal method without addition of surfactant. The unique nanostructures with electrically conductive graphene and ultrafine SnO_2 are favorable for the fast diffusions of lithium ions in SnO_2 lattice and transport of electrons in graphene support during the charge-discharge processes. Hence, the SnO_2-G-400 exhibits a very high reversible capacity of 1037 mAh g^{-1}, excellent capacity retention of 90 % over 150 cycles and good high-rate capability. It is believed that such a simple, economic, and friendly synthesis protocol can be further extended to synthesis of other ultrafine electrochemically active metal oxide-graphene composites to improve the electrochemical performances of lithium-ion batteries.

Acknowledgements

Support of this work by National Natural Science Foundation of China (U1401248) is acknowledged.

References

1. S. B. Yang, G. L. Cui, S. P. Pang, Q. Cao, U. Kolb, X. L. Feng, J. Maier and K. Mullen, *Chemsuschem*, 2010, 3, 236-239.
2. L. Zhi, Y. S. Hu, B. E. Hamaoui, X. Wang, I. Lieberwirth, U. Kolb, J. Maier and K. Müllen, *Adv. Mater.*, 2008, 20, 1727-1731.
3. C. Wang, G. Du, K. Ståhl, H. Huang, Y. Zhong and J. Z. Jiang, *The Journal of Physical Chemistry C*, 2012, 116, 4000-4011.
4. S. B. Yang, X. L. Feng, S. Ivanovici and K. Mullen, *Angew. Chem. Int. Ed.*, 2010, 49, 8408-8411.
5. C. Wang, Y. Zhou, M. Y. Ge, X. B. Xu, Z. L. Zhang and J. Z. Jiang, *J. Am. Chem. Soc.*, 2010, 132, 46-47.
6. J. S. Zhou, L. L. Ma, H. H. Song, B. Wu and X. H. Chen, *Electrochem. Commun.*, 2011, 13, 1357-1360.
7. Y. H. Chang, J. Li, B. Wang, H. Luo, H. Y. He, Q. Song and L. J. Zhi, *J. Mater. Chem. A*, 2013, 1, 14658-14665.
8. J. H. Zhu, J. Jiang, W. Ai, Z. X. Fan, X. T. Huang, H. Zhang and T. Yu, *Nanoscale*, 2014, 6, 12990-13000.
9. J. S. Luo, J. L. Liu, Z. Y. Zeng, C. F. Ng, L. J. Ma, H. Zhang, J. Y. Lin, Z. X. Shen and H. J. Fan, *Nano Lett.*, 2013, 13, 6136-6143.
10. C. Z. Yuan, H. B. Wu, Y. Xie and X. W. Lou, *Angew. Chem. Int. Ed.*, 2014, 53, 1488-1504.
11. J. S. Chen and X. W. Lou, *Small*, 2013, 9, 1877-1893.
12. H. K. Zhang, H. H. Song, X. H. Chen, J. S. Zhou and H. J. Zhang, *Electrochim. Acta*, 2012, 59, 160-167.
13. J. Liang, X. Y. Yu, H. Zhou, H. B. Wu, S. Ding and X. W. D. Lou, *Angewandte Chemie International Edition*, 2014, 53, 12803-12807.
14. C. Guan, X. H. Wang, Q. Zhang, Z. X. Fan, H. Zhang and H. J. Fan, *Nano Lett.*, 2014, 14, 4852-4858.
15. Q. Guo, Z. Zheng, H. L. Gao, J. Ma and X. Qin, *J. Power Sources*, 2013, 240, 149-154.
16. X. Zhou, Z. Dai, S. Liu, J. Bao and Y. G. Guo, *Adv. Mater.*, 2014, 26, 3943-3949.
17. H. Sun, Z. Xu and C. Gao, *Adv. Mater.*, 2013, 25, 2554-2560.
18. Y. Q. Sun, Q. O. Wu and G. Q. Shi, *Energy Environ. Sci.*, 2011, 4, 1113-1132.
19. X. Huang, Z. Y. Zeng, Z. X. Fan, J. Q. Liu and H. Zhang, *Adv. Mater.*, 2012, 24, 5979-6004.
20. W. Sun and Y. Wang, *Nanoscale*, 2014, 6, 11528-11552.
21. C. M. Chen, Q. Zhang, J. Q. Huang, W. Zhang, X. C. Zhao, C. H. Huang, F. Wei, Y. G. Yang, M. Z. Wang and D. S. Su, *J. Mater. Chem.*, 2012, 22, 13947-13955.
22. S. Jiang, B. Zhao, R. Ran, R. Cai, M. O. Tadé and Z. Shao, *Rsc Adv*, 2014, 4, 9367.
23. Y. X. Wang, Y. G. Lim, M. S. Park, S. L. Chou, J. H. Kim, H. K. Liu, S. X. Dou and Y. J. Kim, *J. Mater. Chem. A*, 2014, 2, 529.
24. C. T. Hsieh, W. Y. Lee, C. E. Lee and H. Teng, *The Journal of Physical Chemistry C*, 2014, 118, 15146-15153.
25. Y. H. Hwang, E. G. Bae, K. S. Sohn, S. Shim, X. Song, M. S. Lah and M. Pyo, *J. Power Sources*, 2013, 240, 683-690.
26. X. Liu, J. Cui, J. Sun and X. Zhang, *Rsc Adv*, 2014, 4, 22601.
27. H. K. Kim, S. H. Park, S. B. Yoon, C. W. Lee, J. H. Jeong, K. C. Roh and K. B. Kim, *Chem. Mater.*, 2014, 26, 4838-4843.
28. B. Luo and L. J. Zhi, *Energy Environ. Sci.*, 2015, 8, 456-477.
29. J. Tang, J. Yang, L. Zhou, J. Xie, G. Chen and X. Zhou, *J. Mater. Chem. A*, 2014, 2, 6292.
30. S. B. Yang, X. L. Feng, L. Wang, K. Tang, J. Maier and K. Müllen, *Angew. Chem. Int. Ed.*, 2010, 49, 4795-4799.
31. Y. J. Gong, S. B. Yang, Z. Liu, L. L. Ma, R. Vajtai and P. M. Ajayan, *Adv. Mater.*, 2013, 25, 3979-3984.
32. J. W. S. Hummers and R. E. Offeman, *J. Am. Chem. Soc.*, 1958, 80, 1339.
33. P. Cao, L. Wang, Y. Xu, Y. Fu and X. Ma, *Electrochim. Acta*, 2015, 157, 359-368.
34. T. Rath and P. P. Kundu, *Rsc Adv*, 2015, 5, 26666-26674.
35. S. B. Yang, L. J. Zhi, K. Tang, X. L. Feng, J. Maier and K. Mullen, *Adv. Funct. Mater.*, 2012, 22, 3634-3640.
36. N. A. Kaskhedikar and J. Maier, *Adv. Mater.*, 2009, 21, 2664-2680.
37. B. Huang, J. Yang and X. Zhou, *J. Solid State Electrochem.*, 2014, 18, 2443-2449.
38. M. Shahid, N. Yesibolati, M. C. Reuter, F. M. Ross and H. N. Alshareef, *J. Power Sources*, 2014, 263, 239-245.
39. J. Liang, Z. Cai, Y. Tian, L. Li, J. Geng and L. Guo, *ACS Appl Mater Interfaces*, 2013, 5, 12148-12155.

40. S. Yang, H. Song and X. Chen, *Electrochem. Commun.*, 2006, 8, 137-142.
41. S. Yang, X. Feng, L. Zhi, Q. Cao, J. Maier and K. Müllen, *Adv. Mater.*, 2010, 22, 838-842.